In Silico Exploration of Phytoconstituents From *Phyllanthus emblica* and *Aegle marmelos* as Potential Therapeutics Against SARS-CoV-2 RdRp

$SAGE

Khushboo Pandey[1*], Kiran Bharat Lokhande[1*] (iD),
K Venkateswara Swamy[1,2], Shuchi Nagar[1]
and Manjusha Dake[3] (iD)

[1]Bioinformatics Research Laboratory, Dr. D. Y. Patil Biotechnology & Bioinformatics Institute, Dr. D. Y. Patil Vidyapeeth, Pune, India. [2]Bioinformatics and Drug Discovery Group, MIT School of Bioengineering Sciences & Research, MIT Art, Design and Technology University, Pune, India. [3]Protein Biochemistry Laboratory, Dr. D. Y. Patil Biotechnology & Bioinformatics Institute, Dr. D. Y. Patil Vidyapeeth, Pune, India.

ABSTRACT: Severe acute respiratory syndrome coronavirus 2 (SARS-CoV-2) worldwide has increased the importance of computational tools to design a drug or vaccine in reduced time with minimum risk. Earlier studies have emphasized the important role of RNA-dependent RNA polymerase (RdRp) in SARS-CoV-2 replication as a potential drug target. In our study, comprehensive computational approaches were applied to identify potential compounds targeting RdRp of SARS-CoV-2. To study the binding affinity and stability of the phytocompounds from *Phyllanthus emblica* and *Aegel marmelos* within the defined binding site of SARS-CoV-2 RdRp, they were subjected to molecular docking, 100 ns molecular dynamics (MD) simulation followed by post-simulation analysis. Furthermore, to assess the importance of features involved in the strong binding affinity, molecular field-based similarity analysis was performed. Based on comparative molecular docking and simulation studies of the selected phytocompounds with SARS-CoV-2 RdRp revealed that EBDGp possesses a stronger binding affinity (−23.32 kcal/mol) and stability than other phytocompounds and reference compound, Remdesivir (−19.36 kcal/mol). Molecular field-based similarity profiling has supported our study in the validation of the importance of the presence of hydroxyl groups in EBDGp, involved in increasing its binding affinity toward SARS-CoV-2 RdRp. Molecular docking and dynamic simulation results confirmed that EBDGp has better inhibitory potential than Remdesivir and can be an effective novel drug for SARS-CoV-2 RdRp. Furthermore, binding free energy calculations confirmed the higher stability of the SARS-CoV-2 RdRp-EBDGp complex. These results suggest that the EBDGp compound may emerge as a promising drug against SARS-CoV-2 and hence requires further experimental validation.

KEYWORDS: *Phyllanthus emblica*, *Aegle marmelos* SARS-CoV-2 RdRp, drug repurposing, molecular docking, MD simulation

Introduction

COVID-19 has been referred to as SARS-CoV-2 by the World Health Organization (WHO) in the year 2019.[1] The virus belonging to the order Nidovirales and genus Beta-coronavirus[2,3] has imposed a major challenge in front of human society due to global health concerns. The disease has become pandemic worldwide due to the human-to-human transmission cycle of such a pathogenic virus. The disease originated in China in 2019 has now spread across all over countries with around 170 426 245 confirmed cases of COVID-19, including 3 548 628 deaths as reported by WHO (https://covid19.who.int/) on the date June 1, 2021.

Several targets currently being focused on for identifying novel inhibitors include SARS-CoV-2 spike protein, Angiotensin-converting enzyme-2 (ACE-2), human proteases including transmembrane protease, Serine 2 (TMPRSS2), furin and viral proteases like RNA-dependent RNA polymerase, papain like proteases-2 (PLpro), and main protease

(Mpro).[4-10] Two types of proteins, ie, structural and non-structural proteins characterizing human coronaviruses (HCoVs). SARS-CoV-2, structural proteins include Spike (S), Nucleocapsid (N), Matrix (M), and Envelope (E), whereas non-structural proteins include Nsp1 up to Nsp16[11,12] along with the RNA-dependent RNA polymerase (RdRp) also known as Nsp12.[13,14] The RdRp, a vital enzyme in the life cycle of RNA viruses, has been targeted in various viral infections including Hepatitis C virus (HCV), Zika virus (ZIKV), West Nile virus, and Japanese encephalitis virus (JEV).[15-26] RdRp, a protein crucial for viral replication is a promising druggable antiviral target for coronavirus.[27] RdRp of SARS-CoV-2 supports the transcription and replication of a large RNA genome with approximately 30 000 nucleotides[28-30] and is the most highly conserved protein among RNA viruses.[31] RdRp activity is dependent on magnesium ions and requires the non-structural proteins Nsp7 and Nsp8 for complete activity.[32] Nucleotide and nucleoside analogs inhibiting the action of RNA polymerases would be considered promising antiviral agents.[33] Compounds showing broad-spectrum antiviral

---

*Khushboo Pandey and Kiran Bharat Lokhande contributed equally.

Table 1. List of phytocompounds from *Phyllanthus emblica* and *Aegle marmelos*.

S. NO.	PLANT SOURCE	COMPOUNDS	PUBCHEM CID
1.	*Phyllanthus emblica*	Chebulagic acid[60]	442674
		Pedunculagin[60]	442688
		(2S)-Eriodictyol 7-O-(6''-O-galloyl)-beta-D glucopyranoside (EBDGp)[62]	442688
2	*Aegle marmelos*	Seselin[60]	68229
		Marmelide[48]	10212

activities with their proven action against coronaviruses are under focus. Several such compounds are being evaluated through random clinical trials[34,35] where Remdesivir (RDV) is used5 in the form of a common substrate of several viral RdRp enzymes.[36-39] Remdesivir was approved by the U.S. Food and Drug Administration (US-FDA) on May 1, 2020 for emergency use to treat COVID-19.[40]

Nowadays, phytochemicals are the key sources of antiviral drugs with minimal side effects and therefore are of global interest to identify and explore their potency to treat SARS-CoV-2 viral disease.[41] The extracts derived from medicinal plants have been found to inhibit replication of HSV-2,[42] HIV,[43,44] HBV,[45,46] and SARS-CoV-2 virus.[47] The current approach is the screening of bioactive compounds from medicinal plants, *Aegle marmelos* and *Phyllanthus emblica* that have been already reported to show antiviral activities against Human coxsackieviruses B1-B6, and herpes simplex virus, respectively.[48-50] The *Aegle marmelos* being an important medicinal plant with several bioactive compounds such as Seselin, Aeglein, Marmelide, and Marmelosin is chosen for antiviral study against SARS-CoV-2.[51-55] Some *Phyllanthus species* also exhibit inhibitory potential against HBV, HCV, HIV, and HSV[56-58] and *Phyllanthus emblica* against respiratory syndrome virus (PRRSV).[59] Chebulagic Acid, Pedunculagin, Azadirachtin, and Nimbolide may act as potential inhibitors of the SARS-CoV-2 ACE2 receptor and Mpro.[60] Seselin showed efficacy against multiple targets of SARS-COV-2 such as spike protein and Mpro.[61] However, evidence of these compounds for the treatment of COVID-19 is lacking. Therefore, these compounds were studied for their inhibitory action against SARS-CoV-2 RdRp.

In the present study, *in silico* approach was employed to identify the therapeutic potential of a set of phytocompounds from *Aegle marmelos* and *Phyllanthus emblica* against SARS-CoV-2 RdRp. The potential of these phytocompounds (Table 1) was accessed by performing molecular docking and dynamic simulation studies for analyzing their binding affinity with SARS-CoV-2 RdRp. The molecular field-based similarity of Remdesivir with the obtained lead compound has been employed. The efficacy of these compounds has been compared with Remdesivir for experimental COVID-19 therapy.

Materials and Methods

Preparation of SARS–CoV–2 RdRp structure

The SARS-CoV-2 RdRp structure complexed with an RNA template, and Nsp7, and Nsp8 cofactors crystallized using electron microscopy at 2.93 Å resolution has been selected as a target for the current study. This complex was downloaded from Protein Data Bank with PDB ID: 7C2K.[62]

The receptor structure was prepared using the Protein Preparation Wizard tool of the Maestro program (Schrodinger Release 2020-3: Maestro) at pH 7.5. Removal of water molecules and zinc ion bound with the SARS-CoV-2 RdRp complex along with the subsequent addition of all missing hydrogen atoms and disulfide bonds was carried out. To prevent charge repulsion from the free termini and ensure conformational stability of the protein, N-termini and C-termini of the SARS-CoV-2 RdRp were capped with N-acetyl and N-methyl amide groups respectively. Finally, the prepared and minimized structure of SARS-CoV-2 RdRp was subjected to further docking and molecular dynamic simulation studies.

Phytocompounds retrieval and preparation

To identify promising SARS-CoV-2 RdRp inhibitors, a set of 5 bioactive phytocompounds reported for their antiviral activity, and Remdesivir, a standard reference molecule was retrieved from the PubChem database (https://pubchem.ncbi.nlm.nih.gov/).[63] To get the energetically stable conformation of the retrieved compounds, the energy minimization was performed using the Maestro program with the OPLS3e force field. The most stable conformation having low energy for each compound was used for the docking calculation. The phytocompounds and Remdesivir with their PubChem IDs are enlisted in Table 1.

Defining the binding site of the SARS–CoV–2 RdRp

From the literature study, amino acid residues like Phe441, Asp452, Tyr455, Tyr456, Lys545, Ala547, Arg553, Arg555, Thr556, Ala558, Tyr619, Cys622, Asp623, Arg624, Thr680, Thr687, and Asp760[11,64] are important for ligand binding
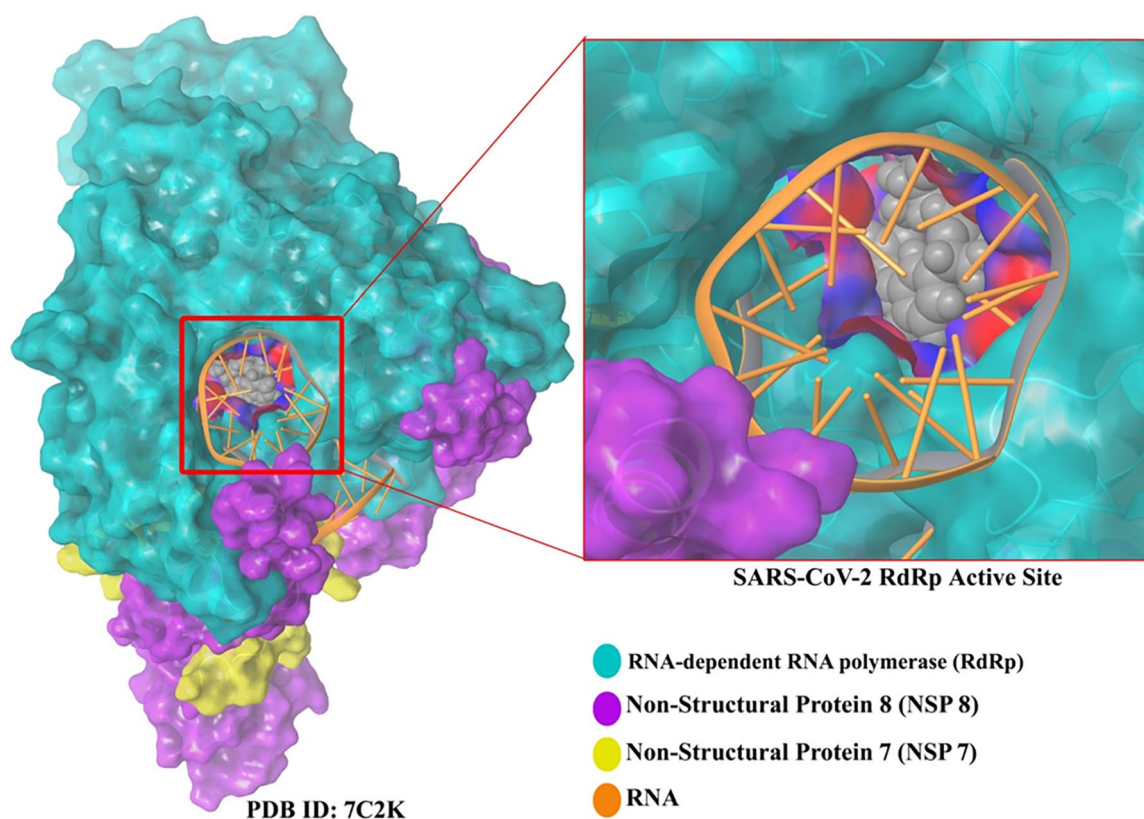
Figure 1. The defined binding pocket of SARS-CoV-2-RdRp (PDB ID: 7C2K). The complex of RdRp (Teal), NSP 8 (Purple), NSP 7 (Yellow), and RNA (Orange) represented with molecular surface and the active site of RdRp shown by CPK representation.
NSP indicates non-structural proteins; PDB, Protein Data Bank; SARS-CoV-2, severe acute respiratory syndrome coronavirus 2; RdRp, RNA-dependent RNA polymerase.

within the SARS-CoV2 RdRp cavity were selected as binding site residues for the docking study (Figure 1).

Molecular docking studies

To study the mode of interactions of phytocompounds in the defined binding site of SARS-CoV-2 RdRp, molecular docking was performed using FlexX software (LeadIT 2.3.2).[65,66] This software uses an incremental buildup algorithm guiding the flexible placement of ligand in the binding region.[67] FlexX considers ligand flexibility by changing the conformations of the ligand in the active site while making the protein rigid.[68] It is an extremely fast, robust, and highly configurable computer program for predicting protein-ligand interactions.[69] The SDF file of the compounds was uploaded in FlexX as a docking library. FlexX default docking parameters were kept with 200 conformations per iteration and maintained conformation per fragmentation. The top-ranked poses were selected for the interaction study, the FlexX rank the resulting docked poses as per the FlexX score (docking energy). The intermolecular interactions between the SARS-CoV-2 RdRp and ligands were studied using the Maestro program (Schrodinger Release 2020-3: Maestro). Binding poses of the ligands visualized in Maestro were selected for further studies based on their binding affinity and mode of interactions with SARS-CoV-2 RdRp. Subsequently, the compounds were subjected to 100 ns MD simulation to probe the binding stability.

Molecular dynamics simulation

To assess the dynamic behavior and binding stability of the docked compounds in the binding cavity of the SARS-CoV-2 RdRp, 100 ns of MD simulation was carried out using the Desmond[70] module of Schrodinger software (Schrodinger Release 2020-3: Desmond). The docked complexes were solvated using an implicit solvent model in a cubic box of 10 Å spacing. The solvated systems were neutralized with counter ions, and physiological salt concentration was maintained to 0.15 M.[71] All the systems were set up at constant NPT (N[number], P[pressure], T[time]) ensemble[72] with atmospheric pressure (1.013 bar), and a constant temperature of 300k over 100 ns simulation.[73]

The systems were minimized and equilibrated with the default settings of relaxation with a time step of 2 fs. The OPLS3e force field was designated to the protein-ligand complex systems.[74] The results were analyzed using MD trajectories generated during 100 ns simulation as root mean square deviation (RMSD), root mean square fluctuation (RMSF), and protein-ligand interactions. Protein-ligand interactions were recorded throughout the 100 ns MD simulation and examined various intermolecular interactions between SARS-CoV-2 RdRp and lead compounds. The protein-ligand interaction profile was normalized throughout the trajectory wherein, the binding site residues were provided that are interacted with SARS-CoV-2 RdRp by various types of interactions.

Binding-free energy calculation (Prime MM/ GBSA)

The molecular mechanics generalized born and surface area (MM/GBSA approach) was used to compute the binding-free energies of the complex system using the Prime module.[75] MM/GBSA is a method to calculate binding energy, which uses energy properties of free ligand, free receptor, and receptor-ligand complex for binding affinity calculation. The more negative MM/GBSA score indicates the formation of more stable protein-ligand complexes.[76,77] We have computed the MM/GBSA from the entire trajectory of the MD simulation run using the trajectory clustering method for each SARS-CoV-2 RdRp complex system. For this purpose, we have taken the entire 100 ns trajectory of MD simulation and extracted the coordinate file at every 10 ns interval. From these, we have calculated the ensemble-averaged binding-free energies (MM/GBSA) value. The free energy of binding can be calculated as

$$\Delta G_{bind} = \Delta H - T\Delta S$$

$\Delta H = \Delta E_{elec} + \Delta E_{vdW} + \Delta G_{polar} + \Delta G_{non-polar}$, where ΔE_{elec} and ΔE_{vdW} are the electrostatic and van der Waal's contributions and G_{polar} and $G_{non-polar}$ are the polar and non-polar solvation terms, respectively.[78-80]

Molecular field-based similarity analysis

FieldTemplater, a component of Forge-Cresset software,[81] was used to perform a conformational search using the extended electron distribution (XED) force field. The technique uses "field points" as a simple and effective descriptor of the electrostatic and van der Waals maxima and minima surrounding a molecule equipped with XED charges.[82,83] Compound with the best binding energy and mode of interactions was selected. The processing was performed using default parameters for the generation of a bioactive field template with a single common field pattern reflecting the binding requirements of the selected compound and Remdesivir.

Results and Discussion

Intermolecular interactions between Remdesivir, EBDGp, and SARS-CoV-2 RdRp

The detailed intermolecular interactions analysis is summarized in Table 2. The binding energy obtained for Remdesivir with SARS-CoV-2 RdRp is –19.36 kcal/mol. The analysis of intermolecular interaction between Remdesivir and SARS-CoV-2 RdRp is showing hydrogen bond interactions with the reported crucial residues Thr556 and Asp623 of SARS-CoV-2 RdRp[11,64] with the bond distance of 2.22 and 2.08 Å, respectively. As per the observation of docking interactions shown in Figure 2A, the -NH group adjacent to the Phosphate group in the structure of Remdesivir is forming hydrogen bond interaction with the carboxylic oxygen atom

of Asp623 amino acid of SARS-CoV-2 RdRp. The carboxylic oxygen atom of Thr556 is hydrogen-bonded with the hydroxyl group of Remdesivir. Hydrogen bonding interactions are also observed with Asp452, Cys622, and Arg624 of SARS-CoV-2 RdRp.

The binding energy obtained for EBDGp with SARS-CoV-2 RdRp is –23.32 kcal/mol. The intermolecular interaction of EBDGp with SARS-CoV-2 RdRp is showing hydrogen bond interactions with the same crucial amino acids Thr556 and Asp623 as observed with Remdesivir. The carboxylic oxygen atom of amino acids Thr556 and Asp623 forms hydrogen bond interactions with the hydroxyl group of EBDGp as shown in Figure 2B with the bond distance of 1.99 and 1.60 Å, respectively. Thr556 of SARS-CoV-2 RdRp forms similar molecular interactions with both Remdesivir and EBDGp. It can be deduced from the above results that EBDGp is showing a similar mode of interactions with amino acid residues Thr556 and Asp623 as Remdesivir despite Asp623 is forming interactions with Remdesivir and EBDGp with different functional groups but forming the similar type of intermolecular interactions, ie, Hydrogen bond. In addition, Asp452, Arg555, Tyr619, Cys622, Thr687, and Asp760 are also involved in hydrogen bond interactions with EBDGp.

Intermolecular interactions between Marmelide, Seselin, and SARS-CoV-2 RdRp

The Marmelide shows the binding energy of –10.30 kcal/mol which is observed to be lower than that of Remdesivir and EBDGp. Interactions of Marmelide with SARS-CoV-2 RdRp are shown in Figure 3A. Hydroxyl group of Marmelide shows to form hydrogen bond interaction with an amino group of Thr556 (2.02 Å) and the secondary amino group of Arg624 with a bond distance of 1.79 Å. Six carbon aromatic ring of Seselin is forming a π-cation bond with the secondary amino group of Arg553 (3.04 Å) and the side-chain amino group of Lys621 (5.85 Å), and backbone amino group of Cys622 (1.98 Å) forms a hydrogen bond with the carbonyl oxygen atom of the Seselin (Figure 3B).

Intermolecular interactions between Pedunculagin, Chebulagic acid, and SARS-CoV-2 RdRp

Pedunculagin and Chebulagic acid show the lowest binding energies (–1.57 and 1.64 kcal/mol, respectively) among all the docked compounds. Interactions of Pedunculagin and Chebulagic acid with SARS-CoV-2 RdRp are shown in Figure 4A and B, respectively. Hydroxyl groups of Pedunculagin forms 2 hydrogen bonds with a carboxylic group of crucial amino acid, ie, Thr556 with a bond distance of 1.57 Å and 2.05 Å. Carbonyl oxygen of Pedunculagin forming a hydrogen bond with an amino group of Cys622 with a bond distance of 1.91 Å. Besides, Arg553 and Lys621 are also forming hydrogen

Table 2. Binding affinity of phytocompounds with the target SARS-CoV2 RdRp.

| SR.NO.	COMPOUND NAME	COMPOUNDS CID	BINDING ENERGY (KCAL/MOL)	INTERACTING RESIDUES	BOND TYPE	BOND DISTANCE (Å)
1.	Remdesivir	121304016	−19.36	**Thr556**[a]	H bond	2.22
				Arg624	H bond	2.09, 1.92
				Asp623[a]	H bond	2.08
				Cys622[a]	H bond	2.07
				Asp452	H bond	1.83
2.	EBDGp	10930068	−23.32	**Thr556**[a]	H bond	1.99
				Arg555	π-cation	6.57
				Asp623[a]	H bond	1.60
				Asp452	H bond	1.76, 1.68
				Cys622[a]	H bond	2.33
				Tyr619	H bond	2.06
				Asp760	H bond	1.49, 2.07
				Thr687	H bond	2.09, 2.76
3.	Marmelide	10212	−10.30	**Thr556**[a]	H bond	2.02
				Arg624	H bond	1.79
4.	Seselin	68229	−10.1	Lys621	π-Cation	5.85
				Arg553	π-Cation	3.04
				Cys622[a]	H bond	1.98
5.	Pedunculagin	442688	−1.57	**Cys622**[a]	H bond	1.91
				Lys621	H bond	2.39
				Arg553	H bond	1.62
				Thr556[a]	H bond	1.57, 2.05
				Asp760	H bond	1.78
6.	Chebulagic acid	442674	1.64	Arg555	H-bond	2.26
				Arg553	π-cation Salt bridge	4.30 2.87
				Arg624	H bond Salt bridge	2.10 3.08
				Asp623[a]	H bond	0.59
				Cys621	H bond	2.76
				Asp760	H bond	1.69
				Tyr619	H bond	2.60

Abbreviations: SARS-CoV-2, severe acute respiratory syndrome coronavirus 2; RdRp, RNA-dependent RNA polymerase.
[a]Common interacting residues with SARS-CoV-2 RdRp.

bond interactions with Pedunculagin. Chebulagic acid shows hydrogen bond interactions with amino acids, namely, Arg553, Arg555, Lys621, Arg624, Thr619, Asp623, and Asp760. The carboxylic group of crucial amino acid Asp623 makes hydrogen bond interaction with the hydroxyl group of Chebulagic acid.

Dynamic behavior of Remdesivir and lead compounds with SARS-CoV-2 RdRp
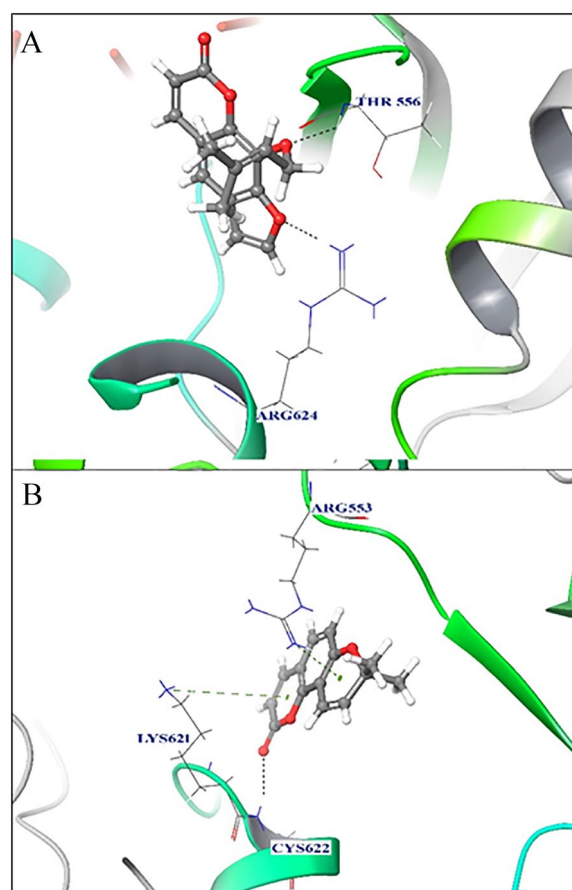
To evaluate the dynamic behavior, 100 ns simulation runs for the docked compounds including Remdesivir in the defined binding pocket of SARS-CoV-2-RdRp was carried out. The information
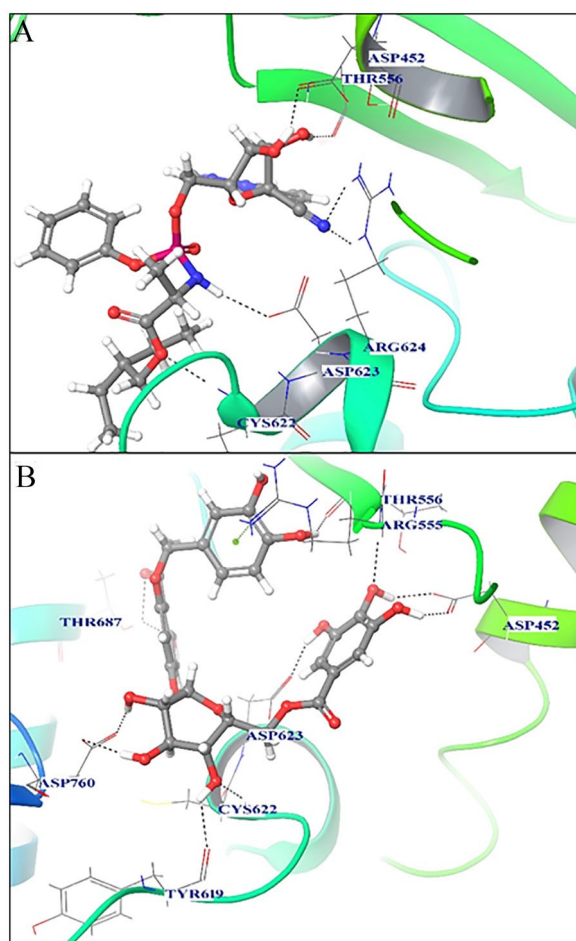
Figure 2. Binding interaction of (A) Remdesivir and (B) EBDGp with SARS-CoV-2 RdRp. Interacting residues are represented in lines and ligand shown in the ball and stick model. Hydrogen bonds are represented by black dashed lines.
SARS-CoV-2 indicates severe acute respiratory syndrome coronavirus 2; RdRp, RNA-dependent RNA polymerase.
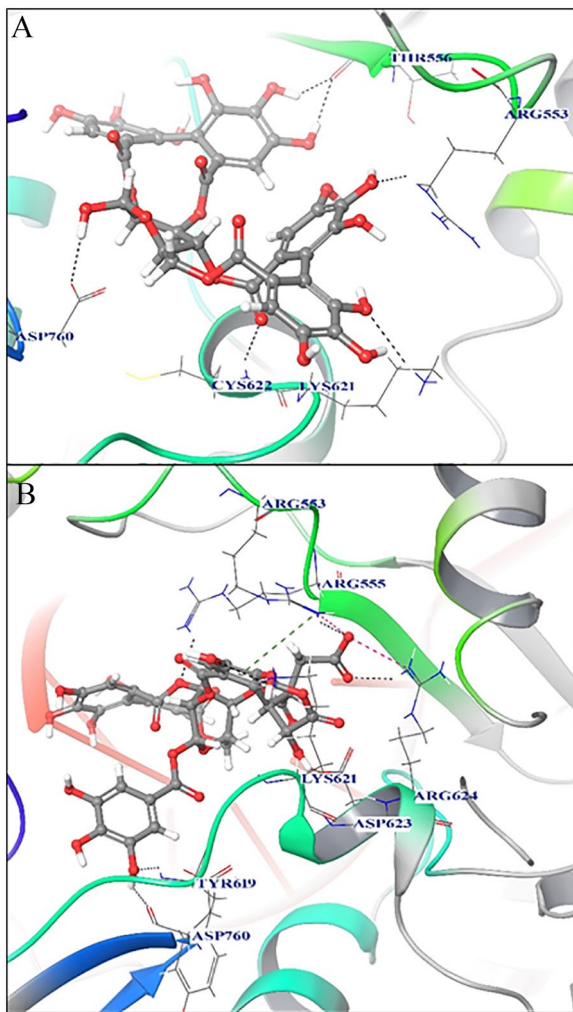

Figure 3. Binding interaction of (A) Marmelide and (B) Seselin with SARS-CoV-2 RdRp. Interacting residues are represented in lines and ligand shown in the ball and stick model. Hydrogen bonds and π-cation are black and green colored dashed lines, respectively.
SARS-CoV-2 indicates severe acute respiratory syndrome coronavirus 2; RdRp, RNA-dependent RNA polymerase.

about the structural stability of the protein-ligand complex could be analyzed by RMSD. Root mean square deviation calculations were performed using changes in C-alpha atoms of SARS-CoV-2-RdRp in complex with docked phytocompounds.

In each complex, it appears that stable equilibrium was reached after 5 ns. The RMSD was observed within 4.5 Å RMSD for the receptor in complex with Seselin, Marmelide, Pedunculagin, and Chebulagic acid throughout the simulation. These compounds have been shown to have lower RMSD values as compared with Remdesivir. Among these compounds, EBDGp was observed to have the lowest RMSD value below 1.5 Å where Remdesivir deviates within the RMSD range of 1.5 to 2.0 Å suggesting higher stability as compared with other phytocompounds and Remdesivir (Figure 5B). However, it can be seen that the receptor is least stable when in complex with Remdesivir, as shown by its highest RMSD (Figure 5A). The Ligand RMSD analysis shows that there is a less deviation of EBDGp (RMSD-1.25 Å) from the binding pocket of the receptor thus showing its role in the overall higher stability of SARS-CoV-2 RdRp as compared with Remdesivir (RMSD-2.25 Å). To further understand the dynamics of the backbone

atoms, the RMSF values were calculated for backbone atoms at each point of the trajectories. Higher RMSF values indicate greater flexibility during the MD simulation.[84]

Low RMSF values (<1.5 Å) of active site residues for all SARS-CoV-2 RdRp-complexes indicate their higher stabilities during the entire MD simulation (Figure 6), signifying that there are no major conformational changes seen in the binding pocket of the SARS-CoV-2 RdRp in complex with all the compounds. Also, RMSF values for the binding pocket residues (C-α atoms) were summarized in Table 3. The RMSF of the SARS-CoV-2 RdRp binding site residues, upon binding of lead compounds, ie, EBDGp, Marmelide Seselin Pedunculagin, and Chebulagic acid is lower than 1 Å, which suggest that the SARS-CoV-2 RdRp binding pocket is more stable with minimum fluctuation during the 100 ns MD simulation.

Intermolecular interaction profile between Remdesivir, lead compounds, and SARS-CoV-2 RdRp

To understand the binding pocket stability, the MD trajectories captured for all systems were superimposed and analyzed using the Simulation Event Analysis tool of Desmond. Figures 7 and 8
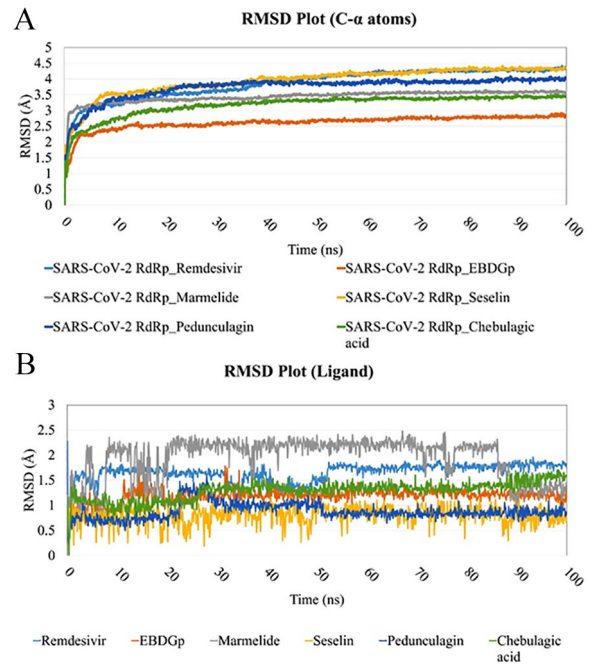
Figure 4. Binding interaction of (A) Pedunculagin and (B) Chebulagic acid with SARS-CoV-2 RdRp. Interacting residues are represented in lines and ligand shown in the ball and stick model. Hydrogen bonds, salt bridge, and π-cation are black, pink, and green colored dashed lines, respectively.
SARS-CoV-2 indicates severe acute respiratory syndrome coronavirus 2; RdRp, RNA-dependent RNA polymerase.
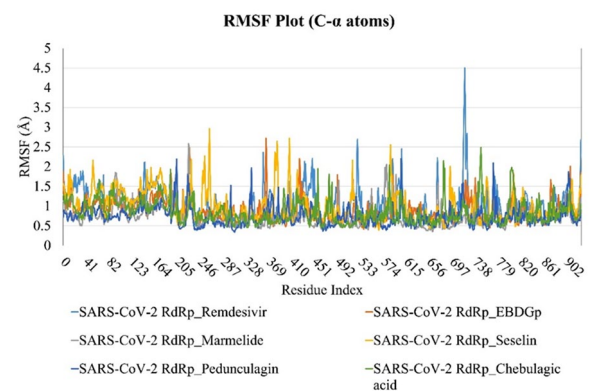

Figure 5. Plots of RMSD of (A) SARS-CoV-2-RdRp C-alpha atoms and (B) lead compounds along with Remdesivir during 100 ns MD simulation time. MD indicates molecular dynamics; SARS-CoV-2, severe acute respiratory syndrome coronavirus 2; RdRp, RNA-dependent RNA polymerase; RMSD, root mean square deviation.

Figure 6. RMSF profiles of the SARS-CoV-2 RdRp complexed with Remdesivir and lead compounds in the entire 100 ns MD simulation. MD indicates molecular dynamics; SARS-CoV-2, severe acute respiratory syndrome coronavirus 2; RdRp, RNA-dependent RNA polymerase; RMSF, root mean square fluctuation.

show interacting residues of SARS-CoV-2 RdRp with the Remdesivir and lead compound during 100 ns MD simulation. Some residues make more than one specific contact with the ligand, which is represented by a darker shade of orange, according to the scale to the right of the plot. Remdesivir, Pedunculagin, EBDGp, and Chebulagic acid are showing good interactions with some active site residues.

Hydrogen bond interaction analysis of the Remdesivir and phytocompounds with SARS-CoV-2 RdRp

To reveal the binding stability between SARS-CoV-2 RdRp and phytocompounds like EBDGp, Marmelide, Seselin, Pedunculagin, and Chebulagic acid, hydrogen bond monitoring was done using the resulting MD trajectories from 100 ns simulation via Simulation Event Analysis module of Maestro. The plots of the hydrogen bonding profile are presented in

Figure 9. In Figure 9A, it is observed that the Remdesivir is making 8 hydrogen bonds with the active site residues of SARS-CoV-2 RdRp such as Asp623 and Asp760 throughout the 100 ns MD simulation. Interestingly, EBDGp is making the highest contacts, ie, about 10 hydrogen bonds as shown in Figure 9B till 25 ns and is observed to maintain 8-10 hydrogen bond contacts with the active site residues such as Asp452, Cys622, Asp623, and Thr680 throughout the 100 ns MD simulation, which is observed to be the highest as compared with a reference compound, Remdesivir. Whereas, other phytocompounds such as Marmelide, Seselin, Pedunculagin, and Chebulagic acid are shown to have the least hydrogen bond contacts as compared with all the other phytocompounds as

Table 3. RMSF values of the amino acids (C-α atoms) which are involved in the SARS-CoV-2 RdRp binding pocket after binding of lead compounds and Remdesivir.

RESIDUES	REMDESIVIR	EBDGP	MARMELIDE	SESELIN	PEDUNCULAGIN	CHEBULAGIC ACID
Phe441	1.573	0.728	0.548	0.615	0.619	0.468
Asp452[a]	1.115	0.756	0.535	0.652	0.832	0.907
Tyr455	0.898	0.777	0.481	0.593	0.503	0.981
Tyr456	0.766	0.776	0.660	0.572	0.558	1.947
Lys545	0.944	0.714	0.427	0.579	0.587	0.801
Ala547	1.132	0.637	0.487	0.496	0.496	0.693
Arg553[a]	1.240	0.845	0.874	0.658	0.595	0.958
Arg555[a]	0.880	0.713	0.674	0.503	0.475	0.615
Thr556[a]	0.867	0.794	0.556	0.728	0.503	0.630
Ala558	0.605	0.676	0.602	0.450	0.590	0.974
Tyr619[a]	0.794	0.635	0.625	0.897	0.541	0.498
Lys621[a]	0.676	0.982	0.575	0.908	0.626	0.664
Cys622[a]	0.720	0.735	0.546	0.784	0.520	0.825
Asp623[a]	0.943	0.655	0.465	0.705	0.431	0.714
Arg624[a]	0.634	0.973	0.501	0.618	0.771	0.551
Thr680	0.508	0.859	0.437	0.620	0.706	1.030
Thr687[a]	0.683	0.498	0.554	0.536	0.445	0.762
Asp760[a]	0.962	0.759	0.514	1.536	0.429	0.482

Abbreviations: SARS-CoV-2, severe acute respiratory syndrome coronavirus 2; RdRp, RNA-dependent RNA polymerase; RMSF, root mean square fluctuation.
[a]Interacting residues of SARS-CoV-2 RdRp with lead compounds and Remdesivir.

can be seen in Figure 9C to F, respectively. From these results, we can conclude that the screened lead compound EBDGp forms a stable complex with SARS-CoV-2 RdRp and thus obtain the complex stability during the 100 ns MD simulation. It is observed that EBDGp is making the highest hydrogen bond contacts for a longer period with most of the active site residues as compared with Remdesivir and other phytocompounds which shows its greater potential in inhibiting SARS-CoV-2 RdRp as compared with Remdesivir.

*Binding free energies for Remdesivir and EBDGp with SARS-CoV-2 RdRp*

To compute binding free energies (ΔG Bind) of protein-ligand complexes, MM/GBSA calculations were performed, which gives the output in the context of VDW, hydrophobic, and solvation components. The phytocompounds and reference compound, Remdesivir, within the binding cavity of SARS-CoV-2 RdRp was subjected to ensemble-averaged Prime MM/GBSA calculations. The resulting free binding energies of each complex by taking ensemble-average MM/GBSA are summarized in Table 4.

Based on the MM/GBSA values obtained, as reported in Table 4, the EBDGp is expected to have a strong binding affinity (−66.498 kcal/mol) as compared with other phytocompounds. However, Remdesivir shows binding free energy of −49.492 kcal/mol with SARS-CoV-2 RdRp. The binding free energy calculation signifies that EBDGp has the most favorable binding free energy (−66.498 kcal/mol) closely followed by Marmelide (−57.145 kcal/mol) as shown in Figure 10. Binding free energy calculations of the compounds reveal that EBDGp forms a stronger and highly stable complex with the SARS-CoV-2 RdRp and all computed energies are found to be thermodynamically favorable as compared with other both phytocompounds and Remdesivir.

Molecular field–based similarity analysis

To evaluate the importance of features involved in the strong binding affinity of EBDGp toward SARS-CoV-2 RdRp, we have performed molecular field-based similarity analysis using FieldTemplater software. It provides the necessary 3D-molecular field properties of the EBDGp in alignment with the Reference molecule, Remdesivir. FieldTemplater took
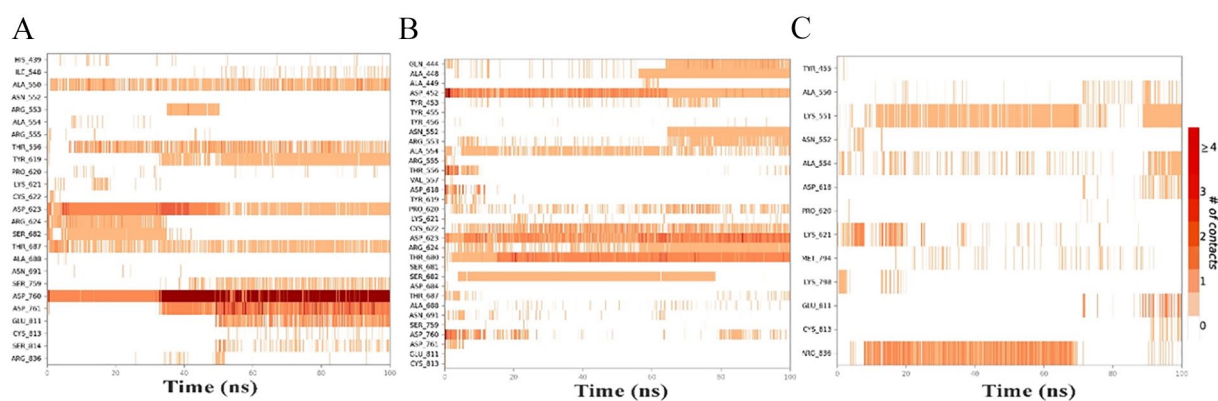
Figure 7. SARS-CoV-2-RdRp interactions profile with (A) Remdesivir, (B) EBDGp, and (C) Marmelide during 100 ns simulation.
SARS-CoV-2 indicates severe acute respiratory syndrome coronavirus 2; RdRp, RNA-dependent RNA polymerase.
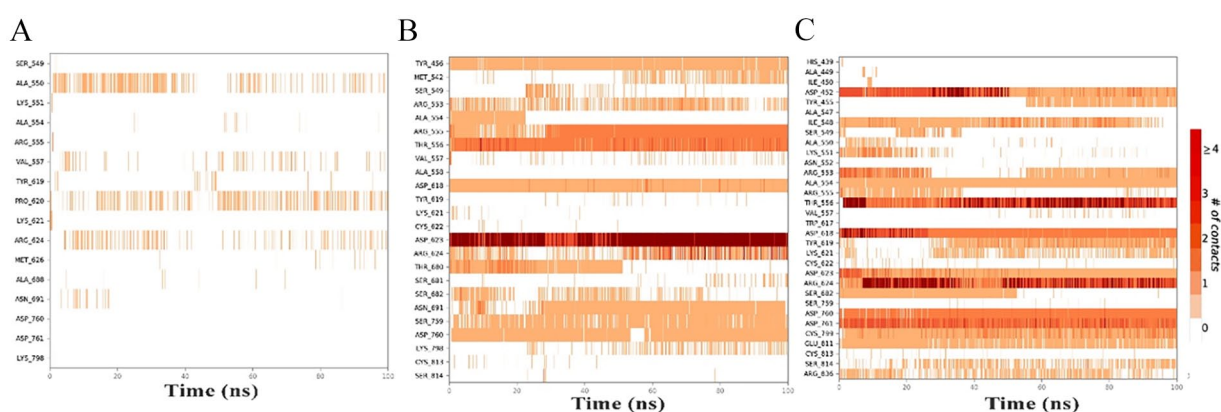
Figure 8. SARS-CoV-2-RdRp interactions profile with (A) Seselin, (B) Pedunculagin, and (C) Chebulagic acid during 100 ns simulation.
SARS-CoV-2 indicates severe acute respiratory syndrome coronavirus 2; RdRp, RNA-dependent RNA polymerase.

2 compounds EBDGp and Remdesivir, optimally aligned their conformer fields, and yielded 89 templates ranked as per incorporated score (Structural similarity, Field similarity, and Shape similarity). The top-ranked molecular field template is presented in Figure 11. In this study, we have explored only common fields with the aligned templates of Remdesivir and EBDGp describing electrostatic (positive and negative), Hydrophobic, and van der Waals properties.

Large points indicating strong interactions as observed in field point patterns,[85] abundant in positive and negative electrostatic fields were observed in Remdesivir and EBDGp. Positive electrostatic fields are seen along with the hydroxyl group of EBDGp and amino group of Remdesivir, but interestingly the positive electrostatic fields are seen in large points along with hydroxyl groups of EBDGp. Large points of negative electrostatic fields are observed along with the carbonyl group and hydrophobic field along the benzoyl aromatic ring of both Remdesivir and EBDGp. Moreover, Van der Waals fields are also abundant along both Remdesivir and EBDGp equally. These results of molecular field-based similarity analysis show that positive electrostatic fields are largely observed along with hydroxyl groups of the EBDGp which indicates the importance of hydroxyl groups in an efficient binding with SARS-CoV-2 RdRp. This study demonstrates that the presence of the

hydroxyl group can be assessed further for lead optimization and the design of a more potent lead candidate.

Conclusions

The present study aimed to test the inhibition potency of 5 phytocompounds from *Phyllanthus emblica* and *Aegel marmelos* against SARS-CoV-2 RdRp using a computational approach. Molecular docking studies were conducted to compare binding affinities toward SARS-CoV-2 RdRp. Only one of them (EBDGp) showed higher FlexX docking energy values than other phytocompounds and a reference molecule, Remdesivir. EBDGp showed strong hydrogen bond interaction with key amino acid residues Thr556 and Asp623. The RMSD and RMSF profiles corresponding to the SARS-CoV-2 RdRp-EBDGp complex suggested that it is highly stable and experienced low conformational fluctuations. The RMSF values for the binding pocket residues of SARS-CoV-2 RdRp, upon binding of phytocompounds, was lower than 1.0 Å, thus it reveals that the binding pocket of SARS-CoV-2 RdRp was very stable during MD simulations. The protein-ligand interaction profile analysis revealed that EBDGp exhibited good interactions with the surrounded amino acid residues throughout the simulation. The pre (after docking study) and post (after MD simulation) MM/GBSA analysis of the EBDGp
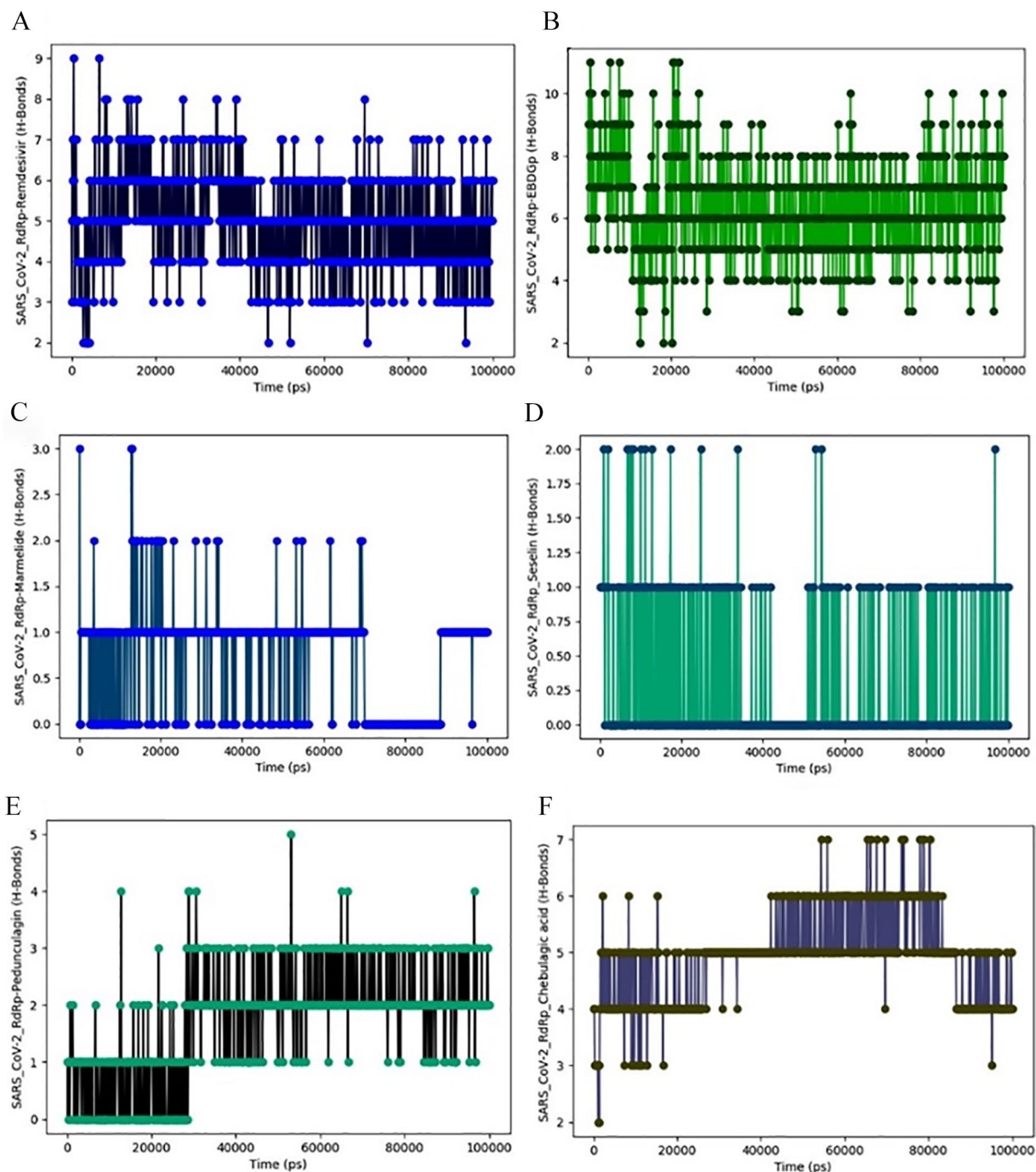
Figure 9. Hydrogen bonding profile of SARS-CoV-2 RdRp with (A) Remdesivir, (B) EBDGp, (C) Marmelide, (D) Seselin, (E) Pedunculagin, and (F) Chebulagic acid during 100 ns simulation.
SARS-CoV-2 indicates severe acute respiratory syndrome coronavirus 2; RdRp, RNA-dependent RNA polymerase.

Table 4. The ensemble-average Prime binding free energies (kcal/mol) of docked complexes during the 100 ns MD simulation.

LEAD COMPOUNDS COMPLEXED WITH SARS-COV-2S RDRP	ΔG BIND[a] (KCAL/MOL)	ΔG BIND COULOMB[b] (KCAL/MOL)	ΔG BIND LIPO[c] (KCAL/MOL)	ΔG BIND SOLV GB[d] (KCAL/MOL)	ΔG BIND VDW[e] (KCAL/MOL)
Remdesivir	−49.492	−17.452	−9.452	30.854	−52.830
	±4.700	±12.150	±1.502	±8.552	±5.803

(Continued)

Table 4. (Continued)

LEAD COMPOUNDS COMPLEXED WITH SARS-COV-2S RDRP	ΔG BIND[a] (KCAL/MOL)	ΔG BIND COULOMB[b] (KCAL/MOL)	ΔG BIND LIPO[c] (KCAL/MOL)	ΔG BIND SOLV GB[d] (KCAL/MOL)	ΔG BIND VDW[e] (KCAL/MOL)
EBDGp	−66.498	−42.547	−9.074	49.440	−48.418
	±2.619	±14.407	±1.482	±7.150	±4.748
Marmelide	−57.145	−33.670	−7.569	32.040	−39.696
	±4.506	±24.894	±1.280	±7.538	±4.260
Seselin	−32.399	−41.354	−10.269	30.923	−34.461
	±2.859	±5.746	±1.024	±4.850	±2.266
Pedunculagin	−25.681	−44.190	−10.053	30.622	−35.925
	±3.175	±4.459	±1.134	±5.082	±4.689
Chebulagic acid	−24.464	−45.851	−9.413	29.695	−35.777
	±2.804	±4.141	±1.110	±3.717	±5.252

Abbreviations: MD, molecular dynamics; SARS-CoV-2, severe acute respiratory syndrome coronavirus 2; RdRp, RNA-dependent RNA polymerase.
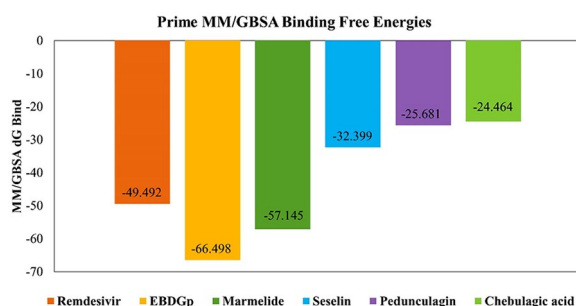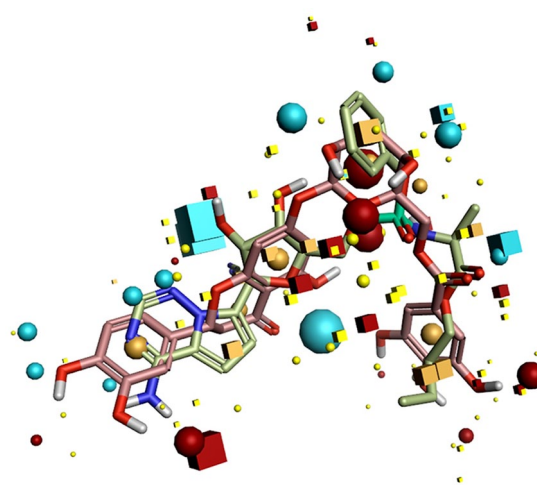[a]MM/GBSA binding free energy.
[b]Coulomb energy.
[c]Lipophilic energy.
[d]Generalized born solvation energy.
[e]Van der Waal energy.

Figure 10. The ensemble-averaged Prime binding free energies in kcal/mol of docked complexes during the 100 ns MD simulation.
MD indicates molecular dynamics; MM/GBSA, molecular mechanics generalized born and surface area.

Figure 11. Field-based template aligned structures of Remdesivir and EBDGp. Field points color coding: negative electrostatic field, blue; positive electrostatic field, red; van der Waal (VDW) surface, yellow; hydrophobic field, orange.

showed higher binding affinity than other phytocompounds and Remdesivir with SARS-CoV-2 RdRp target protein.

Furthermore, molecular field-based similarity profiling has supported our study in the validation of the importance of the presence of hydroxyl groups in EBDGp, increasing its binding affinity with crucial amino acid residues, Thr556 and Asp623 of SARS-CoV-2 RdRp.

This novel concept has percolated the new idea to design and develop promising drugs for effective binding resulting in inhibition of SARS-CoV-2 RdRp. Our study proves that the EBDGp can be a promising SARS-CoV-2 RdRp inhibitor by contributing to its stable and better interactions in the binding pocket of SARS-CoV-2 RdRp for a greater simulation time than that of Remdesivir. Our study for the first time reports the stabilized interactions of phytocompound EBDGp from *Phyllanthus emblica* with SARS-CoV-2 RdRp and confirmed

the role of EBDGp as an anti-SARS-CoV-2 RdRp drug for treating the COVID-19. In the future, biological evaluation can be done to access the therapeutic potential of EBDGp against SARS-CoV-2 RdRp for proceeding to clinical trials.

Author Contributions

The authors confirm contribution to the paper as follows: Study conception and design: MD; data collection: KP, KBL; analysis and interpretation of results: KBL, KP, MD; draft manuscript preparation: KP, KBL, MD; analysis of the data and critical reading and comments: KVS, SN. All authors reviewed the results and approved the final version of the manuscript.

Consent for Publication

All authors approved the final version of the manuscript and the authorship list.

ORCID iD

Kiran Bharat Lokhande (iD) https://orcid.org/0000-0001-6945-8288
Manjusha Dake (iD) https://orcid.org/0000-0001-5578-4939

Availability of Data and Material

All data generated or analyzed during this study are included in this article.

REFERENCES

1. Ji W, Wang W, Zhao X, Zai J, Li X. Cross-species transmission of the newly identified coronavirus 2019-nCoV. *J Med Virol*. 2020;92:433-440. doi:10.1002/jmv.25682.
2. Zheng J. SARS-CoV-2: an emerging coronavirus that causes a global threat. *Int J Biol Sci*. 2020;16:1678-1685. doi:10.7150/ijbs.45053.
3. Elzupir AO. Caffeine and caffeine-containing pharmaceuticals as promising inhibitors for 3-chymotrypsin-like protease of SARS-CoV-2 [published online ahead of print October 23, 2020]. *J Biomol Struct Dyn*. doi:10.1080/07391102.2020.1835732.
4. Andersen KG, Rambaut A, Lipkin WI, Holmes EC, Garry RF. The proximal origin of SARS-CoV-2. *Nat Med*. 2020;26:450-452. doi:10.1038/s41591-020-0820-9.
5. Bestle D, Heindl MR, Limburg H, et al. TMPRSS2 and furin are both essential for proteolytic activation and spread of SARS-CoV-2 in human airway cells and provide promising drug targets [published online ahead of print April 15, 2020]. *bioRxiv*. doi:10.1101/2020.04.15.042085.
6. Coutard B, Valle C, de Lamballerie X, Canard B, Seidah NG, Decroly E. The spike glycoprotein of the new coronavirus 2019-nCoV contains a furin-like cleavage site absent in CoV of the same clade. *Antiviral Res*. 2020;176:104742. doi:10.1016/j.antiviral.2020.104742.
7. Hoffmann M, Kleine-Weber H, Schroeder S, et al. SARS-CoV-2 cell entry depends on ACE2 and TMPRSS2 and is blocked by a clinically proven protease inhibitor. *Cell*. 2020;181:210-271. doi:10.1016/j.cell.2020.02.052.
8. Walls AC, Park YJ, Tortorici MA, Wall A, McGuire AT, Veesler D. Structure, function, and antigenicity of the SARS-CoV-2 spike glycoprotein. *Cell*. 2020;181:281-292. doi:10.1016/j.cell.2020.02.058.
9. Xia S, Liu M, Wang C, et al. Inhibition of SARS-CoV-2 (previously 2019-nCoV) infection by a highly potent pan-coronavirus fusion inhibitor targeting its spike protein that harbors a high capacity to mediate membrane fusion. *Cell Res*. 2020;30:343-355. doi:10.1038/s41422-020-0305-x.
10. Xia S, Zhu Y, Liu M, et al. Fusion mechanism of 2019-nCoV and fusion inhibitors targeting HR1 domain in spike protein. *Cell Mol Immunol*. 2020;17:765-767. doi:10.1038/s41423-020-s0374-2.
11. Ahmad M, Dwivedy A, Mariadasse R, et al. Prediction of small molecule inhibitors targeting the severe acute respiratory syndrome coronavirus-2 RNA-dependent RNA polymerase. *ACS Omega*. 2020;5:18356-18366. doi:10.1021/acsomega.0c02096.
12. Mangar P, Pradhan S, Rai S, Lepcha K, Ranjan VK. Comparative analysis based on the spike glycoproteins of SARS-CoV2 isolated from COVID 19 patients of different countries [published online ahead of print April 9, 2020]. *Preprints*. doi:10.20944/preprints202004.0154.v1.
13. Elfiky AA, Mahdy SM, Elshemey WM. Quantitative structure-activity relationship and molecular docking revealed a potency of anti-hepatitis C virus drugs against human corona viruses. *J Med Virol*. 2017;89:1040-1047. doi:10.1002/jmv.24736.
14. Hasan A, Paray BA, Hussain A, et al. A review on the cleavage priming of the spike protein on coronavirus by angiotensin-converting enzyme-2 and furin. *J Biomol Struct Dyn*. 2021;39:3025-3033. doi:10.1080/07391102.2020.1754293.
15. Elfiky AA. Zika viral polymerase inhibition using anti-HCV drugs both in market and under clinical trials. *J Med Virol*. 2016;88:2044-2051. doi:10.1002/jmv.24678.
16. Elfiky AA. Zika virus: novel guanosine derivatives revealed strong binding and possible inhibition of the polymerase. *Future Virol*. 2017;12:721-728. doi:10.2217/fvl-2017-0081.
17. Elfiky AA. Novel guanosine derivatives as anti-HCV NS5b polymerase: a QSAR and molecular docking study. *Med Chem*. 2019;15:130-137. doi:10.2174/1573406414666181015152511.
18. Elfiky AA, Elshemey WM, Gawad WA, Desoky OS. Molecular modeling comparison of the performance of NS5b polymerase inhibitor (PSI-7977) on prevalent HCV genotypes. *Protein J*. 2013;32:75-80. doi:10.1007/s10930-013-9462-9.
19. Elfiky AA, Elshemey WM. IDX-184 is a superior HCV direct acting anti-viral drug: a QSAR study. *Med Chem Res*. 2016;25:1005-1008. doi:10.1007/s00044-016-1533-y.
20. Elfiky AA, Elshemey WM. Molecular dynamics simulation revealed binding of nucleotide inhibitors to ZIKV polymerase over 444 nanoseconds. *J Med Virol*. 2018;90:13-18.
21. Elfiky AA, Ismail A. Molecular dynamics and docking reveal the potency of novel GTP derivatives against RNA dependent RNA polymerase of genotype 4a HCV. *Life Sci*. 2019;238:116958. doi:10.1016/j.lfs.2019.116958.
22. Elfiky AA, Ismail AM. Molecular modeling and docking revealed superiority of IDX-184 as HCV polymerase inhibitor. *Future Virol*. 2017;12:339-347. doi:10.2217/fvl-2017-0027.
23. Ganesan A, Barakat K. Applications of computer-aided approaches in the development of hepatitis C antiviral agents. *Expert Opin Drug Discov*. 2017;12:407-425. doi:10.1080/17460441.2017.1291628.
24. Mercorelli B, Palù G, Loregian A. Drug repurposing for viral infectious diseases: how far are we? *Trends Microbiol*. 2018;26:865-876. doi:10.1016/j.tim.2018.04.004.
25. Lee G, Piper DE, Wang Z, et al. Novel inhibitors of hepatitis C virus RNA-dependent RNA polymerases. *J Mol Biol*. 2006;357:1051-1057. doi:10.1016/j.jmb.2006.01.032.
26. Lim SP, Noble CG, Seh CC, et al. Potent allosteric dengue virus NS5 polymerase inhibitors: mechanism of action and resistance profiling. *PLoS Pathog*. 2016;12:e1005737. doi:10.1371/journal.ppat.1005737.
27. Riccio F, Talapatra SK, Oxenford S, Angell R, Mazzon M, Kozielski F. Development and validation of RdRp screen, a crystallization screen for viral RNA-dependent RNA polymerases. *Biol Open*. 2019;8:bio037663. doi:10.1242/bio.037663.
28. Grum-Tokars V, Ratia K, Begaye A, Baker SC, Mesecar AD. Evaluating the 3C-like protease activity of SARS-coronavirus: recommendations for standardized assays for drug discovery. *Virus Res*. 2008;133:63-73. doi:10.1016/j.virusres.2007.02.015.
29. Marra MA, Jones SJ, Astell CR, et al. The genome sequence of the SARS-associated coronavirus. *Science*. 2003;300:399-1404. doi:10.1126/science.1085953.
30. Thiel V, Ivanov KA, Putics A, et al. Mechanisms and enzymes involved in SARS coronavirus genome expression. *J Gen Virol*. 2003;84:2305-2315. doi:10.1099/vir.0.19424-0.
31. Jacome R, Campillo-Balderas JA, Ponce-De Leon S, Becerra A, Lazcano A. Sofosbuvir as a potential alternative to treat the SARS-CoV-2 epidemic. *Sci Rep*. 2020;10:9294. doi:10.21203/rs.3.rs-21002/v1.
32. Kirchdoerfer RN, Ward AB. Structure of the SARS-CoV nsp12 polymerase bound to nsp7 and nsp8 co-factors. *Nat Commun*. 2019;10:2343. doi:10.1038/s41467-019-10280-3.
33. Debing Y, Neyts J, Delang L. The future of antivirals: broad-spectrum inhibitors. *Curr Opin Infect Dis*. 2015;28:596-602. doi:10.1097/QCO.0000000000000212.
34. Li H, Zhou Y, Zhang M, Wang H, Zhao Q, Liu J. Updated approaches against SARS-CoV-2. *Antimicrob Agents Chemother*. 2020;64:e00483-20. doi:10.1128/AAC.00483-20.
35. Siegel D, Hui HC, Doerffler E, et al. Discovery and synthesis of a phosphoramidate prodrug of a pyrrolo[2,1-f][triazin-4-amino] adenine C-nucleoside (GS-5734) for the treatment of Ebola and emerging viruses. *J Med Chem*. 2017;60:1648-1661. doi:10.1021/acs.jmedchem.6b01594.
36. Agostini ML, Andres EL, Sims AC, et al. Coronavirus susceptibility to the antiviral Remdesivir (GS-5734) is mediated by the viral polymerase and the proofreading exoribonuclease. *mBio*. 2018;9:e00221-18. doi:10.1128/mBio.00221-18.

37. Jordan PC, Liu C, Raynaud P, et al. Initiation, extension, and termination of RNA synthesis by a paramyxovirus polymerase. *PLoS Pathog*. 2018;14:e1006889. doi:10.1371/journal.ppat.1006889.

38. Warren TK, Jordan R, Lo MK, et al. Therapeutic efficacy of the small molecule GS-5734 against Ebola virus in rhesus monkeys. *Nature*. 2016;531:381-385. doi:10.1038/nature17180.

39. Tchesnokov EP, Feng JY, Porter DP, Götte M. Mechanism of inhibition of Ebola virus RNA-dependent RNA polymerase by Remdesivir. *Viruses*. 2019;11:326. doi:/10.3390/v11040326.

40. US-Food & Drug Administration. *Fact Sheet for Health Care Providers: Emergency Use Authorization (EUA) of Remdesivir (GS-5734TM)*. Silver Spring, MD: US-Food & Drug Administration; 2020.

41. Mani JS, Johnson JB, Steel JC, et al. Natural product-derived phytochemicals as potential agents against coronaviruses: a review. *Virus Res*. 2020;284:197989. doi:10.1016/j.virusres.2020.197989.

42. Debiaggi M, Pagani L, Cereda PM, Landini P, Romero E. Antiviral activity of Chamaecyparis lawsoniana extract: study with herpes simplex virus type 2. *Microbiologica*. 1988;11:55-61.

43. Asres K, Bucar F. Anti-HIV activity against immunodeficiency virus type 1 (HIV-I) and type II (HIV-II) of compounds isolated from the stem bark of Combretum molle. *Ethiop Med J*. 2005;43:15-20.

44. Vermani K, Garg S. Herbal medicines for sexually transmitted diseases and AIDS. *J Ethnopharmacol*. 2002;80:49-66. doi:10.1016/s0378-8741(02)00009-0.

45. Huang L, Chen CH. Molecular targets of anti-HIV-1 triterpenes. *Curr Drug Targets Infect Disord*. 2002;2:33-36. doi:10.2174/1568005024605936.

46. Kwon DH, Kwon HY, Kim HM, et al. Inhibition of hepatitis B virus by an aqueous extract of Agrimonia eupatoria L. *Phytother Res*. 2005;19:355-358. doi:10.1002/ptr.1689.

47. Kotwal GJ, Kaczmarek JN, Leivers S, et al. Anti-HIV, anti-poxvirus, and anti-SARS activity of a nontoxic, acidic plant extract from the Trifollium species Secomet-V/anti-vac suggests that it contains a novel broad-spectrum antiviral. *Ann N Y Acad Sci*. 2005;1056:293-302. doi:10.1196/annals.1352.014.

48. Badam L, Bedekar SS, Sonawane KB, Joshi SP. In vitro antiviral activity of bael (Aegle marmelos Corr) upon human coxsackieviruses B1-B6. *J Commun Dis*. 2002;34:88-99.

49. Melnick JL. Enterovirus type 71 infections: a varied clinical pattern sometimes mimicking paralytic poliomyelitis. *Rev Infect Dis*. 1984;6:S387-S390. doi:10.1093/clinids/6.supplement_2.s387.

50. Xiang Y, Pei Y, Qu C, et al. In vitro anti-herpes simplex virus activity of 1, 2, 4, 6-tetra-O-galloyl-β-D-glucose from Phyllanthus emblica L. (Euphorbiaceae). *Phytother Res*. 2011;25:975-982. doi:10.1002/ptr.3368.

51. Somu C, Karuppiah H, Sundaram J. Antiviral activity of Seselin from Aegle marmelos against nuclear polyhedrosis virus infection in the larvae of silkworm, Bombyx mori. *J Ethnopharmaco*. 2019;245:112155. doi:10.1016/j.jep.2019.112155.

52. Manandhar MD, Shoeb A, Kapil RS, Popli SP. New alkaloids from Aegle marmelos. *Phytochemistry*. 1978;17:1814-1815.

53. Govindachari TR, Premila MS. Some alkaloids from Aegle marmelos. *Phytochemistry*. 1983;22:755-757.

54. Maity P, Hansda D, Bandyopadhyay U, Mishra DK. Biological activities of crude extracts of chemical constituents of Bael, A. marmelos (L) Corr. *Indian J Exp Biol*. 2009;47:849-861.

55. Farooq S. *555 Medicinal Plants: Field and Laboratory Manual (Identification With Its Phytochemical and In Vitro Studies Data)*. Dehradun, India: International Book Distributors; 2005:318. http://en.wikipedia.org/wiki/Tridax_procumbens.

56. Xiang YF, Pei Y, Wang YF. Current status of natural products from plants as anti-herpes simplex virus 1 agents. *Virol Sin*. 2008;23:305-314.

57. Khan MT, Ather A, Thompson KD, Gambari R. Extracts and molecules from medicinal plants against herpes simplex viruses. *Antiviral Res*. 2005;67:107-119. doi:10.1016/j.antiviral.2005.05.002.

58. Alvarez AL, Dalton KP, Nicieza I, et al. Bioactivity-guided fractionation of Phyllanthus orbicularis and identification of the principal anti HSV-2 compounds. *Phytother Res*. 2012;26:1513-1520. doi:10.1002/ptr.4608.

59. Arjin C, Pringproa K, Hongsibsong S, et al. In vitro screening antiviral activity of Thai medicinal plants against porcine reproductive and respiratory syndrome virus. *BMC Vet Res*. 2020;16:102. doi:10.1186/s12917-020-02320-8.

60. Srivastav AK, Gupta SK, Kumar U. Computational studies towards identification of lead herbal compounds of medicinal importance for development of nutraceutical against COVID-19 [published online ahead of print July 1, 2020]. *ChemRxiv*. doi:10.26434/chemrxiv.12581819.v1.

61. Nivetha R, Bhuvaragavan S, Janarthanan S. Inhibition of multiple SARS-CoV-2 proteins by an antiviral biomolecule, Seselin from Aegle marmelos deciphered using molecular docking analysis [published online ahead of print May 22, 2020]. *Res Sq*. doi:10.21203/rs.3.rs-31134/v1.

62. Wang Q, Wu J, Wang H, et al. Structural basis for RNA replication by the SARS-CoV-2 polymerase. *Cell*. 2020;182:417-428.e13. doi:10.1016/j.cell.2020.05.034.

63. Kim S, Gindulyte A, Zhang J, Thiessen PA, Bolton EE. PubChem periodic table and element pages: improving access to information on chemical elements from authoritative sources. *Chem Teach Int*. 2021;3:57-65. doi:10.1515/cti-2020-0006.

64. Dey SK, Saini M, Dhembla C, et al. Suramin, Penciclovir and Anidulafungin bind nsp12, which governs the RNA-dependent-RNA polymerase activity of SARS-CoV-2, with higher interaction energy than Remdesivir, indicating potential in the treatment of Covid-19 [published online ahead of print April 21, 2020]. *OSF Prepr*. doi:10.31219/osf.io/urxwh.

65. Böhm HJ. Prediction of binding constants of protein ligands: a fast method for the prioritization of hits obtained from de novo design or 3D database search programs. *J Comput Aided Mol Des*. 1998;12:309-323. doi:10.1023/a:1007999920146.

66. Bursulaya BD, Totrov M, Abagyan R, Brooks CL 3rd. Comparative study of several algorithms for flexible ligand docking. *J Comput Aided Mol Des*. 2003;17:755-763. doi:10.1023/b:jcam.0000017496.76572.6f.

67. Srinivasan S, Sadasivam SK, Gunalan S, Shanmugam G, Kothandan G. Application of docking and active site analysis for enzyme linked biodegradation of textile dyes. *Environ Pollut*. 2019;248:599-608. doi:10.1016/j.envpol.2019.02.080.

68. Rarey M, Kramer B, Lengauer T, Klebe G. A fast flexible docking method using an incremental construction algorithm. *J Mol Biol*. 1996;261:470-489. doi:10.1006/jmbi.1996.0477.

69. Kasam V, Salzemann J, Botha M, et al. WISDOM-II: screening against multiple targets implicated in malaria using computational grid infrastructures. *Malar J*. 2009;8:88. doi:10.1186/1475-2875-8-88.

70. Bowers KJ, Chow E, Xu H, et al. Scalable algorithms for molecular dynamics simulations on commodity clusters. Paper presented at: SC '06: Proceedings of the 2006 ACM/IEEE Conference on Supercomputing; November 11-17, 2006; Tampa, FL. doi:10.1145/1188455.1188544.1188544.

71. Kumar BK, Faheem K, Sekhar Ojha R, Prajapati VK, Pai A, Murugesan S. Pharmacophore based virtual screening, molecular docking, molecular dynamics and MM-GBSA approach for identification of prospective SARS-CoV-2 inhibitor from natural product databases [published online ahead of print September 28, 2020]. *J Biomol Struct Dyn*. doi:10.1080/07391102.2020.1824814.

72. Kalibaeva G, Ferrario M, Ciccotti G. Constant pressure-constant temperature molecular dynamics: a correct constrained NPT ensemble using the molecular virial. *Mol Phys*. 2003;101:765-778. doi:10.1080/0026897021000044025.

73. Lokhande KB, Nagar S, Swamy KV. Molecular interaction studies of Deguelin and its derivatives with Cyclin D1 and Cyclin E in cancer cell signaling pathway: the computational approach. *Sci Rep*. 2019;9:1778. doi:10.1038/s41598-018-38332-6.

74. Jorgensen WL, Maxwell DS, Tirado-Rives J. Development and testing of the OPLS all atom force field on conformational energetics and properties of organic liquids. *J Am Chem Soc*. 1996;118:11225-11236. doi:10.1021/ja9621760.

75. Jacobson MP, Pincus DL, Rapp CS, et al. A hierarchical approach to all-atom protein loop prediction. *Proteins*. 2004;55:351-367. doi:10.1002/prot.10613.

76. Kalirajan R, Pandiselvi A, Gowramma B, Balachandran P. In-silico design, ADMET screening, MM-GBSA binding free energy of some novel isoxazole substituted 9-anilinoacridines as HER2 inhibitors targeting breast cancer. *Curr Drug Res Rev*. 2019;11:118-128. doi:10.2174/2589977515666190912154817.

77. Pant R, Joshi A, Maiti P, Nand M, Pande V, Chandra S. Identification of potential mycolyltransferase Ag85C inhibitors of Mycobacterium tuberculosis H37Rv via virtual high throughput screening and binding free energy studies. *J Mol Graph Model*. 2020;98:107584. doi:10.1016/j.jmgm.2020.107584.

78. Ghosh R, Chakraborty A, Biswas A, Chowdhuri S. Potential therapeutic use of corticosteroids as SARS CoV-2 main protease inhibitors: a computational study [published online ahead of print October 23, 2020]. *J Biomol Struct Dyn*. doi:10.1080/07391102.2020.1835728.

79. Lokhande KB, Doiphode S, Vyas R, Swamy KV. Molecular docking and simulation studies on SARS-CoV-2 Mpro reveals Mitoxantrone, Leucovorin, Birinapant, and Dynasore as potent drugs against COVID-19 [published online ahead of print August 20, 2020]. *J Biomol Struct Dyn*. doi:10.1080/07391102.2020.1805019.

80. Lokhande KB, Ballav S, Thosar N, Swamy KV, Basu S. Exploring conformational changes of PPAR-Y complexed with novel kaempferol, quercetin, and resveratrol derivatives to understand binding mode assessment: a small-molecule checkmate to cancer therapy. *J Mol Model*. 2020;26:242. doi:10.1007/s00894-020-04488-0.

81. Laurieri N, Dairou J, Egleton JE, et al. From arylamine N-acetyltransferase to folate-dependent acetyl CoA hydrolase: impact of folic acid on the activity of (HUMAN)NAT1 and its homologue (MOUSE)NAT2. *PLoS ONE*. 2014;9:e96370. doi:10.1371/journal.pone.0096370.

82. Cheeseright T, Mackey M, Rose S, Vinter A. Molecular field extrema as descriptors of biological activity: definition and validation. *J Chem Inf Model*. 2006;46:665-676. doi:10.1021/ci050357s.

83. Cheeseright T, Mackey M, Rose S, Vinter A. Molecular field technology applied to virtual screening and finding the bioactive conformation. *Expert Opin Drug Discov*. 2007;2:131-144. doi:10.1517/17460441.2.1.131.

84. Mandour YM, Zlotos DP, Alaraby Salem M. A multi-stage virtual screening of FDA-approved drugs reveals potential inhibitors of SARS-CoV-2 main protease [published online ahead of print October 23, 2020]. *J Biomol Struct Dyn*. doi:10.1080/07391102.2020.1837680.

85. Xing RJ, Wang J, Pan L, Cheng MS. A selective pharmacophore model for beta(2)-adrenoceptor agonists. *Molecules*. 2009;14:4486-4496. doi:10.3390/molecules14114486.